AIMS Mathematics, 8(6): 13432−13453.
DOI: 10.3934/math.2023681
Received: 05 January 2023
Revised: 17 February 2023
Accepted: 01 March 2023
Published: 06 April 2023

http://www.aimspress.com/journal/Math

Research article

Onset of triple-diffusive convective stability in the presence of a heat source and temperature gradients: An exact method

Yellamma[1], N. Manjunatha[1,*], Umair Khan[2,3], Samia Elattar[4], Sayed M. Eldin[5], Jasgurpreet Singh Chohan[6], R. Sumithra[7] and K. Sarada[8]

[1] Department of Mathematics, School of Applied Sciences, REVA University, Bengaluru-560064, India
[2] Department of Mathematical Sciences, Faculty of Science and Technology, Universiti Kebangsaan Malaysia, UKM Bangi 43600, Selangor, Malaysia
[3] Department of Mathematics and Social Sciences, Sukkur IBA University, Sukkur 65200, Sindh Pakistan
[4] Department of Industrial and Systems Engineering, College of Engineering, Princess Nourah bint Abdulrahman University, P.O. Box 84428, Riyadh 11671, Saudi Arabia
[5] Center of Research, Faculty of Engineering, Future University in Egypt, New Cairo 11835, Egypt
[6] Department of Mechanical Engineering and University Centre for Research and Development, Chandigarh University, Mohali-140413, India
[7] Department of UG, PG Studies and Research in Mathematics, Nrupathunga University, Bengaluru-560001, India
[8] Department of Mathematics, Government City College, Hyderabad, India

* **Correspondence:** Email: manjunatha.n@reva.edu.in; Tel: +919686623528.

Abstract: In the current work, in the presence of a heat source and temperature gradients, the onset of triple-diffusive convective stability is studied for a fluid, and a fluid-saturated porous layer confined vertically by adiabatic limits for the Darcy model is thoroughly analyzed. With consistent heat sources in both layers, this composite layer is subjected to three temperature profiles with Marangoni effects. The fluid-saturated porous region's lower boundary is a rigid surface, while the fluid region's upper boundary is a free surface. For the system of ordinary differential equations, the thermal surface-tension-driven (Marangoni) number, which also happens to be the Eigenvalue, is solved in closed form. The three different temperature profiles are investigated, the thermal surface-tension-driven

(Marangoni) numbers are calculated analytically, and the effects of the heat source/sink are studied in terms of corrected internal Rayleigh numbers. Graphs are used to show how different parameters have an impact on the onset of triple-diffusive convection. The study's parameters have a greater influence on porous layer dominant composite layer systems than on fluid layer dominant composite layer systems. Finally, porous parameters and corrected internal Rayleigh numbers are stabilize the system, and solute1 Marangoni number and ratio of solute2 diffusivity to thermal diffusivity of fluid are destabilize the system.

Keywords: triple-diffusive; convective stability; adiabatic boundaries; composite layer; heat source/sink; thermal Marangoni number
Mathematics Subject Classification: 76Rxx, 76R05, 80M30

1. Introduction

The study of non-Newtonian fluids such as the Walters fluid, Rivlin-Ericksen fluid, and pair stress fluid is critically necessary due to the expanding importance of these fluids in various domains such as industries and modern technologies. In convective problems, it is preferable to study fluid flow with free boundaries in the presence of a solute gradient due to the wide range of applications in the ionosphere, astrophysics, and atmospheric physics. Several liquid systems contain more than two components. As a result, the stability of multi-object systems must be considered. Few authors have looked into triple diffusive convection for fluid/porous media [1−4]. Heat generated by chemical reactions in the fluid brought on by radiation from an external medium might result in the development of an internal heat source (sink), which can help speed up or slow down convection. A perturbation approach was used by Raghunatha et al. [5] to study the three-component convection in a porous layer. Patil et al. [6,7] investigate triple diffusive boundary layer flow along an external flow velocity that is exponentially and vertically decreasing. The effects of the magnetic field and heat source on three-component convection in an Oldroyd-B liquid were investigated using the Galerkin method by Gayathri et al. [8]. Archana et al. [9] studied the triple diffusive flow in the presence of nanofluid. Heat transfer has been one of the top contenders to get involved in many applications, which has drawn the attention of many researchers to the study of porous media [10]. Eyring-Powell nanomaterials were examined from the triple diffusion perspective by Khan et al. [11]. The effects triple-diffusive mixed convection was studied numerically by Sushma et al. [12] for Casson fluid. Li et al. [13] studied the double diffusion for nanofluid with mixed convection in the presence of a heat source. They discovered that the viscoelastic parameter and Hartmann number cause the wall shear stress to rise. The triple-mass diffusion for nanoparticle mixes in Carreau-Yasuda material was explored by Sohail et al. [14]. In presence of chemical reaction and heat source, Sharma and Gandhi [15] examined the MHD on heat and mass transmission in a Darcy-Forchheimer porous medium. Using Oldroyd-B type model with heat source, Arshika et al. [16] explored the impact of sinusoidal and nonsinusoidal waveforms on triple diffusive-convection in viscoelastic liquids. Using lie-group transformation, Nagendramma et al. [17] look into the dynamics of triple diffusive convection. They found that the influence of heat and mass transfer rates decreased for both fluid flow scenarios as the Lewis number increased. In the presence of heat source/sink [18−21] and nanofluid [22−26] few authors have attempted to study the

convective stability. The inverse problems in porous media have been studied extensively see [27,28].

Recently, for the composite layers, Manjunatha and Sumithra [29,30] examined the problem of triple component convection in a combined layer for three different temperature profiles with and without a magnetic field and obtained the corresponding thermal Marangoni numbers. The double-diffusive convection in the existence of a heat source and temperature profiles were studied by Manjunatha and Sumithra [31] and Manjunatha et al. [32]. They found that a linear model is unstable and an inverted parabolic model is more stable.

The current work examines the stability of the onset of triple-diffusive convective stability in a fluid and fluid-saturated porous layer in the presence of a constant heat source and uses an exact technique to investigate the effect of temperature gradients on the corresponding thermal Marangoni (surface-tension-driven) numbers. Furthermore, the investigation of non-uniform fundamental temperature gradients at the start is intriguing since it opens up new perspectives on how convective instability is managed. The discussion takes into account the following non-dimensional basic temperature gradients: linear, parabolic, and inverted parabolic temperature profiles. Over a wide range of controlling physical parameters, the eigenvalue problem is analytically resolved using the exact technique. Numerous applications in astronomy, engineering, geophysics, climatology, and crystal formation (see Rudolph et al. [33]) will surely benefit from this work.

2. Materials and methods

Consider horizontally infinite fluid and fluid-saturated porous layers of depth d_f and d_m respectively. The lower rigid surface $z_m = -d_m$ and upper free surface boundary $z = d_f$ are maintained at constant temperature and concentration $T = T_0$ and $C = C_0$. At the upper free region, surface tension (σ_t) force acts which varies linearly with temperature and concentration respectively in the form $\sigma_t = \sigma_0 - \sigma_T \Delta T$ and $\sigma_t = \sigma_0 - \sigma_C \Delta C$. Where $\sigma_T = \frac{-\partial \sigma_t}{\partial T}$, $\sigma_C = \frac{-\partial \sigma_t}{\partial C}$ and σ_0 is the unperturbed value. The fluid-saturated porous medium interface is located at position at $z = 0 = z_m$, and the temperature and concentration difference between the lower and higher bounds is denoted by ΔT and ΔC. A coordinate system is used as shown in Figure 1. The relevant equations with Oberbeck-Boussinesq approximation for two regions as following Roberts [34], Char & Chiang [35], Del Rio & Whitaker [36], Othman [37] and Shivakumara et al. [38,39].

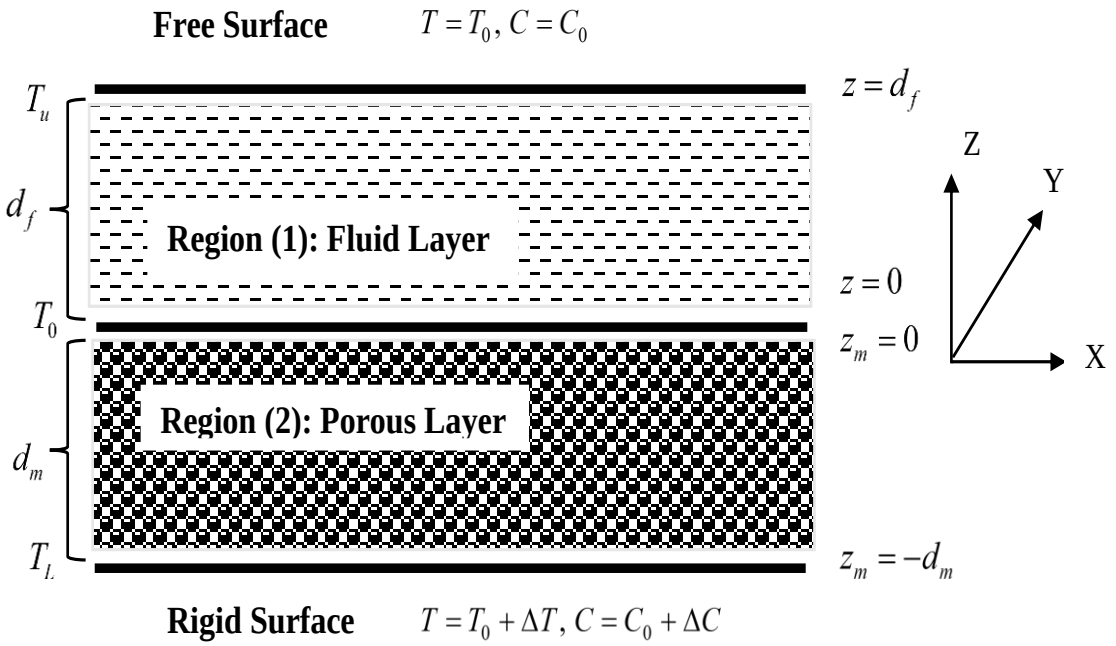

Figure 1. Schematic representation.

Region-1, Fluid layer:

$$\nabla.\vec{q}_f = 0, \tag{1}$$

$$\rho_0\left[\frac{\partial\vec{q}_f}{\partial t} + (\vec{q}_f.\nabla)\vec{q}_f\right] = -\nabla P_f + \mu_f\nabla^2\vec{q}_f, \tag{2}$$

$$\frac{\partial T_f}{\partial t} + (\vec{q}_f.\nabla)T_f = \kappa_f\nabla^2 T_f + Q_f, \tag{3}$$

$$\frac{\partial C_{f1}}{\partial t} + (\vec{q}_f.\nabla)C_{f1} = \kappa_{f1}\nabla^2 C_{f1}, \tag{4}$$

$$\frac{\partial C_{f2}}{\partial t} + (\vec{q}_f.\nabla)C_{f2} = \kappa_{f2}\nabla^2 C_{f2}. \tag{5}$$

Region-2, Porous layer:

$$\nabla_m.\vec{q}_m = 0\ , \tag{6}$$

$$\rho_0\left[\frac{1}{\phi}\frac{\partial\vec{q}_m}{\partial t} + \frac{1}{\phi^2}(\vec{q}_m.\nabla_m)\vec{q}_m\right] = -\nabla_m P_m - \frac{\mu_m}{K}\vec{q}_m, \tag{7}$$

$$M\,\frac{\partial T_m}{\partial t} + (\vec{q}_m.\nabla_m)T_m = \kappa_m\nabla_m^2 T_m + Q_m, \tag{8}$$

$$\phi\frac{\partial C_{m1}}{\partial t} + (\vec{q}_m.\nabla_m)C_{m1} = \kappa_{m1}\nabla_m^2 C_{m1}, \tag{9}$$

$$\phi \frac{\partial C_{m2}}{\partial t} + (\vec{q}_m . \nabla_m) C_{m2} = \kappa_{m2} \nabla_m^2 C_{m2} \ , \tag{10}$$

where the subscript 'f' refers to the fluid layer (region-1) and the subscript 'm' refers to the porous medium (region-2), $\vec{q}_f = (u, v, w), \vec{q}_m = (u_m, v_m, w_m)$ are the velocity vectors, ρ_0 is the reference fluid density, P_f, P_m are the pressures, Q_f, Q_m are the constant heat sources, κ_f, κ_m are the thermal diffusivities, $C_{f1}, C_{f2}, C_{m1}, C_{m2}$ are the salinity field1 and salinity field2, K is the permeability, M is the ratio of heat capacities, ϕ is the porosity, μ_f, μ_m are the fluid viscosities, and $\kappa_{f1}, \kappa_{f2}, \kappa_{m1}, \kappa_{m2}$ are the solute1diffusivities and solute2 diffusivities.

The basic state is quiescent in regions 1 and 2, respectively.

$$\left[\vec{q}_f, P_f, T_f, \chi_f(z), C_{fi}\right] = \left[0, P_{fb}(z), T_{fb}(z), \frac{-dT_b}{dz}, C_{fib}(z)\right], \text{ for } i = 1, 2 \ , \tag{11}$$

$$\left[\vec{q}_m, P_m, T_m, \chi_m(z_m), C_{mi}\right] = \left[0, P_{mb}(z_m), T_{mb}(z_m), \frac{-dT_{mb}}{dz_m}, C_{mib}(z_m)\right], \text{ for } i = 1, 2 \ , \tag{12}$$

The basic state of $T_{fb}(z), T_{mb}(z_m)$, $C_{fib}(z), C_{mib}(z_m)$,for $i = 1, 2$,are

$$-\frac{\partial T_{fb}}{\partial z} = \frac{Q_f z(z - d_f)}{2\kappa_f} + \frac{(T_0 - T_u)}{d_f} \chi_f(z) \ , \ 0 \le z \le d_f \ , \tag{13}$$

$$-\frac{\partial T_{mb}}{\partial z_m} = \frac{Q_m z_m (z_m + d_m)}{2\kappa_m} + \frac{(T_l - T_0)}{d_m} \chi_m(z_m) \ , \ -d_m \le z_m \le 0 \ , \tag{14}$$

$$C_{fib}(z) = C_{i0} - \frac{(C_{i0} - C_{iu})z}{d_f} \ , \ 0 \le z \le d_f \ , \tag{15}$$

$$C_{mib}(z_m) = C_{i0} - \frac{(C_{il} - C_{i0})z_m}{d_m} \ , \ -d_m \le z_m \le 0 \ , \tag{16}$$

where the basic state is denoted by the subscript 'b', $T_0 = \frac{\kappa_f d_m T_u + \kappa_m d_f T_l}{\kappa d_m + \kappa_m d_f} + \frac{d_f d_m (Q_m d_m + Q_f d_f)}{2(\kappa_f d_m + \kappa_m d_f)}$ is the interface temperature, $C_{i0} = \frac{\kappa_{fi} d_m C_{iu} + \kappa_{mi} d_f C_{il}}{\kappa_{fi} d_m + \kappa_{mi} d_f}$ is the interface concentrations for $i = 1, 2$. $\int_0^{d_f} \chi_f(z)\, dz = \frac{\Delta T_f}{d_f}, \int_0^{d_m} \chi_m(z_m))\, dz_m = \frac{\Delta T_m}{d_m}$ are the temperature gradient in region-1 and region-2.

To examine the stability of the system, we perturb the system as

$$\left[\vec{q}_f, P_f, T_f, C_{fi}\right] = \left[\vec{q}_f{}', P_b(z) + P_f', T_{fb}(z) + \theta_f', C_{fib}(z) + C_{fi}'\right], \text{ for } i = 1, 2 \ , \tag{17}$$

$$\left[\vec{q}_m, P_m, T_m, C_{mi}\right] = \left[\vec{q}_m{}', P_b(z) + P_m', T_{mb}(z_m) + \theta_m', C_{mib}(z_m) + C_{mi}'\right], \text{ for } i = 1, 2, \tag{18}$$

where the perturbed primed quantities are those that are very small in relation to the primed quantities of the fundamental state. After substituting Eqs (17) and (18) into Eqs (1–10), linearized in usual manner, eliminate the pressure term from the Eqs (2) and (7) by executing curl twice, and retain the vertical element, the governing stability equations were eventually determined.

Region-1:

$$\frac{1}{P_{rf}}\frac{\partial}{\partial t}\left(\nabla^2 \vec{q}_f\right) = \nabla^4 \vec{q}_f \ , \tag{19}$$

$$\frac{\partial \theta_f}{\partial t} - \left(\chi_f(z) + R_a^*(2z-1)\right)\vec{q}_f = \nabla^2 \theta_f \ , \tag{20}$$

$$\frac{\partial C_{f1}}{\partial t} = \vec{q}_f + \tau_{f1}\nabla^2 C_{f1}, \tag{21}$$

$$\frac{\partial C_{f2}}{\partial t} = \vec{q}_f + \tau_{f2}\nabla^2 C_{f2}, \tag{22}$$

Region-2:

$$\frac{\beta^2}{P_{rm}}\frac{\partial}{\partial t}(\nabla^2 \vec{q}_m) = -\nabla^2 \vec{q}_m \ , \tag{23}$$

$$M\ \frac{\partial \theta_m}{\partial t} - \chi_m(z_m)\vec{q}_m - R_{am}^*(1+2z_m)\vec{q}_m = \nabla^2 \theta_m, \tag{24}$$

$$\phi\frac{\partial C_{m1}}{\partial t} = \vec{q}_m + \tau_{m1}\nabla^2 C_{m1}, \tag{25}$$

$$\phi\frac{\partial C_{m2}}{\partial t} = \vec{q}_m + \tau_{m2}\nabla^2 C_{m2}, \tag{26}$$

here $\nabla^2 = \dfrac{\partial^2}{\partial x^2} + \dfrac{\partial^2}{\partial y^2} + \dfrac{\partial^2}{\partial z^2}$ is the Laplacian operator.

3. Stability analysis and normal mode technique

Establish dimensionless values using standard linear stability analysis methods.

$$\left.\begin{array}{l} (x, y, z) = d_f\left(x^*, y^*, z^*\right),\ \theta' = \Delta T_f\,\theta^*,\ P_f = \dfrac{\mu_f\,\kappa_f}{d_f^2}P^*, \\ (u, v, w) = \dfrac{\kappa}{d_f}\left(u^*, v^*, w^*\right),\ \nabla = \dfrac{1}{d_f}\,\nabla^*,\ t = \dfrac{d_f^2}{\kappa_f}\,t^*, \chi_f(z) = \dfrac{\Delta T_f}{d_f}\,\chi_f(z)^* \end{array}\right\}, \tag{27}$$

$$\left.\begin{array}{l}\left(x_m, y_m, z_m\right)=d_m\left(x_m^{*}, y_m^{*}, z_m^{*}-1\right),\ \theta_m'=\Delta T_m\,\theta_m^{*},\ P_m=\dfrac{\mu_m\,\kappa_m}{d_m^{\,2}}P_m^{*},\\ \left(u_m, v_m, w_m\right)=\dfrac{\kappa_m}{d_m}\left(u^{*}, v^{*}, w^{*}\right),\ \nabla=\dfrac{1}{d_m}\nabla^{*},\ t_m=\dfrac{\phi\, d_m^{\,2}}{\kappa_m}t_m^{*}, \chi_m(z_m)=\dfrac{\Delta T_m}{d_m}\chi(z_m)^{*}\end{array}\right\}, \tag{28}$$

The normal mode approach for the fluid and fluid-saturated porous media respectively,

$$\begin{bmatrix} w' \\ T_f^{'} \\ C_{f1}^{'} \\ C_{f2}^{'} \end{bmatrix} = \begin{bmatrix} W_f(z) \\ \Theta_f(z) \\ \Sigma_{f1}(z) \\ \Sigma_{f2}(z) \end{bmatrix} exp\left[i(\alpha_x x + \alpha_y y) + \varpi t \right], \tag{29}$$

$$\begin{bmatrix} w_m^{'} \\ T_m^{'} \\ C_{m1}^{'} \\ C_{m2}^{'} \end{bmatrix} = \begin{bmatrix} W_m(z_m) \\ \Theta_m(z_m) \\ \Sigma_{m1}(z_m) \\ \Sigma_{m2}(z_m) \end{bmatrix} exp\left[i(\alpha_{xm} x + \alpha_{ym} y) + \varpi_m t \right], \tag{30}$$

where α_x, α_y and α_{xm}, α_{ym} are wavenumbers in x and y direction respectively, and ϖ, ϖ_m are growth rate (real or complex) in region-1 and region-2 respectively.

Nondimensionalized using (27) and (28), and introducing Eqs (29) and (30) into (19)–(26), the equations are becomes

Region-1: $0 \le z_f \le 1$

$$\left(D_f^2 - a_f^2 + \frac{\varpi}{Pr} \right)(D_f^2 - a_f^2) W_f(z) = 0\ , \tag{31}$$

$$(D_f^2 - a_f^2 + \varpi)\Theta_f(z) + [\chi_f(z) + R_a^{*}(2z_f - 1)]W_f(z) = 0\ , \tag{32}$$

$$\left(\tau_{f1}(D_f^2 - a_f^2) + \varpi\right)\Sigma_{f1}(z) + W_f(z) = 0\ , \tag{33}$$

$$\left(\tau_{f2}(D_f^2 - a_f^2) + \varpi\right)\Sigma_{f2}(z) + W_f(z) = 0\ , \tag{34}$$

Region-1: $-1 \le z_m \le 0$

$$\left(1 - \frac{\beta^2 \varpi_m}{P_{rm}} \right)(D_m^2 - a_m^2) W_m(z_m) = 0\ , \tag{35}$$

$$(D_m^2 - a_m^2 + M\varpi_m)\Theta_m(z_m) = -[\chi_m(z_m) + R_{am}^{*}(2z_m + 1)]W_m(z_m)\ , \tag{36}$$

$$\left(\tau_{m1}(D_m^2 - a_m^2) + \varpi_m \phi\right)\Sigma_{m1}(z_m) = -W_m(z_m)\ , \tag{37}$$

$$\left(\tau_{m2}(D_m^2 - a_m^2) + \varpi_m \phi\right)\Sigma_{m2}(z_m) = -W_m(z_m)\ , \tag{38}$$

where $P_r = \frac{\nu_f}{\kappa_f}$, $P_{rm} = \frac{\nu_m}{\kappa_m}$ are the Prandtl numbers and $\beta = \sqrt{\frac{K}{d_m^2}}$ is the square root of Darcy number.

For the current problem, the approach of linear stability analysis and the idea of stability exchange are appropriate and effective so take $\varpi = 0$ and $\varpi_m = 0$. (Refer Manjunatha and Sumithra [30] and Shivakumara et al. [38]).The eigenvalue problem (31)–(38) takes the form.

Region-1: $0 \le z_f \le 1$

$$\left(D_f^2 - a_f^2\right)(D_f^2 - a_f^2)W_f(z) = 0 \ , \tag{39}$$

$$(D_f^2 - a_f^2)\Theta_f(z) + [\chi_f(z) + R_a^*(2z_f - 1)]W_f(z) = 0 \ , \tag{40}$$

$$\left(\tau_{f1}(D_f^2 - a_f^2)\right)\Sigma_{f1}(z) + W_f(z) = 0 \ , \tag{41}$$

$$\left(\tau_{f2}(D_f^2 - a_f^2)\right)\Sigma_{f2}(z) + W_f(z) = 0 \ , \tag{42}$$

Region-1: $-1 \le z_m \le 0$

$$(D_m^2 - a_m^2)W_m(z_m) = 0 \ , \tag{43}$$

$$(D_m^2 - a_m^2)\Theta_m(z_m) = -[\chi_m(z_m) + R_{am}^*(2z_m + 1)]W_m(z_m) \ , \tag{44}$$

$$\left(\tau_{m1}(D_m^2 - a_m^2)\right)\Sigma_{m1}(z_m) = -W_m(z_m) \ , \tag{45}$$

$$\left(\tau_{m2}(D_m^2 - a_m^2)\right)\Sigma_{m2}(z_m) = -W_m(z_m) \ , \tag{46}$$

where, $D_f = \frac{d}{dz}, D_m = \frac{d}{dz_m}$ are the Differential operator, $a_f = \sqrt{\alpha_x{}^2 + \alpha_y{}^2}, a_m = \sqrt{\alpha_{xm}{}^2 + \alpha_{ym}{}^2}$ are the overall horizontal wave numbers, $R_a^* = \frac{R_{If}}{2(T_0 - T_u)}, R_{am}^* = \frac{R_{Im}}{2(T_l - T_0)}$ are the corrected internal Rayleigh numbers, $R_{If} = \frac{Q_f d_f^2}{\kappa_f}, R_{Im} = \frac{Q_m d_m^2}{\kappa_m}$ are the internal Rayleigh numbers, $W_f(z), W_m(z_m)$ are the vertical component of velocities, $\tau_{f1} = \frac{\kappa_{f1}}{\kappa_f}, \tau_{f2} = \frac{\kappa_{f2}}{\kappa_f}$ are the diffusivity ratios, $\tau_{m1} = \frac{\kappa_{m1}}{\kappa_m}, \tau_{m2} = \frac{\kappa_{m2}}{\kappa_m}$ are the diffusivity ratios in porous region, $\Sigma_{f1}(z), \Sigma_{f2}(z)$ are the salinity distributions, $\Sigma_{m1}(z_m), \Sigma_{m2}(z_m)$ are the salinity distributions on porous region, and $\Theta_f(z), \Theta_m(z_m)$ are the amplitude temperatures. For the composite system, the overall horizontal wave numbers must be $a_m = \hat{d}\, a_f$, here $\hat{d} = \frac{d_m}{d_f}$ is the depth ratio.

4. Boundary conditions

The bottom layer is a rigid surface, while the top border is a free surface, with temperature and concentration/salinity affecting surface tension. Prior to applying the normal mode technique, each boundary condition is nondimensionalized (see Sumithra [2]).

$$D_f^2 W_f(z) + M_t a^2 \Theta_f(z) + M_{S1} a^2 \Sigma_{f1}(z) + M_{S2} a^2 \Sigma_{f2}(z) = 0 \ , \text{at } z = 1, \tag{47}$$

$$W_f(z) = 0, W_m(z_m) = 0, D_m W_m(z_m) = 0, \text{ at } z = 1, z_m = -1.$$

$$\left.\begin{aligned} &\hat{T} W_f(z) = W_m(z_m), D_f^2 W_f(z) + a_f^2 W_f(z) = \frac{\hat{\mu}}{\hat{T}\hat{d}^2}\left[D_m^2 W_m(z_m) + a_m^2 W_m(z_m)\right], \\ &\hat{T}\hat{d}^3\beta^2\left[D_f^3 W_f(z) - 3a_f^2 D_f W_f(z)\right] = \left[\hat{\mu}\beta^2(D_m^3 - 3a_m^2 D_m) - D_m\right] W_m(z_m), \end{aligned}\right\} \text{, at } z = 0, z_m = 0,$$

$$\left.\begin{aligned} &D_f \Theta_f(z) = 0, D_m \Theta_m(z_m) = 0, \end{aligned}\right\} \text{, at } z = 1, z_m = -1,$$

$$\left.\begin{aligned} &\Theta_f(z) = \hat{T}\Theta_m(z_m), D_f \Theta_f(z) = D_m \Theta_m(z_m), \end{aligned}\right\} \text{, at } z = 0, z_m = 0,$$

$$\left.\begin{aligned} &D_f \Sigma_{f1}(z) = 0, D_f \Sigma_{f2}(z) = 0, D_m \Sigma_{m1}(z_m) = 0, D_m \Sigma_{m2}(z_m) = 0 \end{aligned}\right\} \text{, at } z = 1, z_m = -1,$$

$$\left.\begin{aligned} &\Sigma_{f1}(z) = \hat{S}_1 \Sigma_{m1}(z_m), D_f \Sigma_{f1}(z) = D_m \Sigma_{m1}(z_m) \\ &\Sigma_{f2}(z) = \hat{S}_2 \Sigma_{m2}(z_m), D_f \Sigma_{f2}(z) = D_m \Sigma_{m2}(z_m) \end{aligned}\right\} \text{, at } z = 0, z_m = 0, \tag{48}$$

where $M_t = \sigma_T \dfrac{\Delta T \ d_f}{\mu_f \kappa_f}$ denotes the thermal Marangoni (surface-tension-driven) number (TMN), $M_{Si} = \dfrac{\sigma_C (C_{iu} - C_{i0}) d_f}{\mu_f \kappa_f}$ for $i = 1, 2$ denotes the solute Marangoni (surface-tension-driven) numbers (SMN's), β is the porous parameter , $\hat{S}_i = \dfrac{C_{il} - C_{i0}}{C_{i0} - C_{iu}}$ for $i = 1, 2$ is the solute diffusivity ratio, $\hat{T}$ is the thermal ratio, and $\hat{\mu} = \dfrac{\mu_m}{\mu_f}$ is the viscosity ratio.

5. Exact method of solution

The eigenvalue problem with an eigenvalue of M_t is formed by the boundary conditions of (48) and the Eqs (39)−(46). We address this problem using the exact technique procedure, which produces acceptable results when dealing with difficulties of this nature (see Manjunatha and Sumithra [29,30]).

5.1. Velocity profiles

The velocity profiles are obtained from Eqs (39) and (43) as follows:

$$W_f(z) = B_1[\cosh a_f z + b_1 z \cosh a_f z + b_2 \sinh a_f z + b_3 z \sinh a_f z] \ , \tag{49}$$

$$W_m(z_m) = B_1[b_4 \cosh a_m z_m + b_5 \sinh a_m z_m] \, , \tag{50}$$

where $b_i's (i = 1, 2, 3, 4, 5)$ need to be calculated utilizing the suitable velocity conditions of (48) yields to $b_1 = \frac{a_m \coth a_m}{2a_f^3 \beta^2 \hat{d}^3}, b_2 = -1 - (b_1 + b_3) \tanh a_f, b_3 = \frac{a_m^2 \hat{\mu} - a_f^2 \hat{d}^2}{a_f \hat{d}^2}, b_4 = \hat{T}, b_5 = \hat{T} \coth a_m.$

5.2. Salinity profiles

Using the solutal boundary conditions (48), the salinity profiles are obtained from Eqs (41), (42), (45) and (46) as follows

$$\Sigma_{f1}(z) = B_1[b_{18}\cosh a_f z + b_{19}\sinh a_f z + g_2(z)]\,, \tag{51}$$

$$\Sigma_{f2}(z) = B_1[b_{22}\cosh a_f z + b_{23}\sinh a_f z + g_3(z)]\,, \tag{52}$$

$$\Sigma_{m1}(z_m) = A_1[b_{20}\cosh a_m z_m + b_{21}\sinh a_m z_m + g_{2m}(z_m)]\,, \tag{53}$$

$$\Sigma_{m2}(z_m) = B_1[b_{24}\cosh a_m z_m + b_{25}\sinh a_m z_m + g_{3m}(z_m)], \tag{54}$$

Where, $g_2(z) = \frac{-z}{4a_f^2\tau_{f1}}\left[\left(2a_f b_1 - b_2 + a_f b_3 z\right)cosh\, a_f z + \left(2a_f - b_3 + a_f b_2 z\right)sinh\, a_f z\right]$,

$g_{2m}(z_m) = \dfrac{-z_m\cosh a_m z_m}{2a_m\tau_{m1}}[(b_5 + b_4\tanh a_m z_m)]$, $b_{18} = \hat{S}_1 b_{20}, b_{19} = \frac{1}{a_f}(b_{21}a_m + \mathbb{N}_1 - \mathbb{N}_2)$,

$b_{20} = \frac{\mathbb{N}_6 a_m\, cosh\, a_m - \mathbb{N}_3\mathbb{N}_5}{a_m\, sinh\, a_m(\mathbb{N}_5 + \mathbb{N}_4\, coth\, a_m)}$, $b_{21} = \frac{\mathbb{N}_3\mathbb{N}_4 + \mathbb{N}_6 a_m\, sinh\, a_m}{a_m\, sinh\, a_m(\mathbb{N}_5 + \mathbb{N}_4\, coth\, a_m)}$,

$g_3(z) = \dfrac{-z}{4a_f^2\tau_{f2}}\left[\left(2a_f b_1 - b_2 + a_f b_3 z\right)\cosh a_f z + \left(2a_f - b_3 + a_f b_2 z\right)\sinh a_f z\right]$,

$g_{3m}(z_m) = \dfrac{-z_m\sinh a_m z_m}{2a_m\tau_{m2}}[(b_5\coth a_m z_m + b_4)]$, $b_{22} = \hat{S}_2 b_{24}, b_{23} = \frac{1}{a_f}(b_{25}a_m + \mathbb{N}_8 - \mathbb{N}_9)$,

$b_{24} = \dfrac{\mathbb{N}_{13}a_m\, cosh\, a_m - \mathbb{N}_{10}\mathbb{N}_{12}}{a_m\, sinh\, a_m\,(\mathbb{N}_{12} + \mathbb{N}_{11}\, coth\, a_m)}$, $b_{25} = \dfrac{\mathbb{N}_{10}\mathbb{N}_{11} + \mathbb{N}_{13}a_m\, sinh\, a_m}{a_m\, sinh\, a_m\,(\mathbb{N}_{12} + \mathbb{N}_{11}\, coth\, a_m)}$.

6. Temperature gradient

We considered linear, parabolic and inverted parabolic profiles, these profiles have been discussed numerically and analytically by Shivakumara et al. [38−40] using the Galerkin procedure for porous layers in absence of heat source and in a linear case by Kaloni and Lou [41] by applying a compound matrix method for single layers. We have revisited these instances in order to determine the analytical reliability of the results for the two layers on the onset of triple-diffusive convection in a fluid and saturated porous layer.

6.1. Model 1: Linear temperature profile: $\chi_f(z) = 1$ *and* $\chi_m(z_m) = 1$

Introducing model into (40) and (44), the linear profile takes the form

$$\Theta_f(z) = B_1[b_6\cosh a_f z + b_7\sinh a_f z + g_1(z)]\,, \tag{55}$$

$$\Theta_m(z_m) = B_1[b_8\cosh a_m z_m + b_9\sinh a_m z_m + g_{1m}(z_m)]\,. \tag{56}$$

From (47), the thermal Marangoni (surface-tension-driven) number (TMN) for the linear model is

$$M_{t1} = \frac{-\Lambda_1 - a_f^2 M_{S1}\Lambda_2 - a_f^2 M_{S2}\Lambda_3}{a_f^2 \Theta_f(1)}\,, \tag{57}$$

where $\Lambda_1 = a_f^2(\cosh a_f + b_1 \sinh a_f) + b_2(a_f^2 \cosh a_f + 2a_f \sinh a_f) + b_3(a_f^2 \sinh a_f + 2a_f \cosh a_f)$,
$\Lambda_2 = [b_{18} \cosh a_f + b_{19} \sinh a_f + g_2(1)],\ \Lambda_3 = [b_{22} \cosh a_f + b_{23} \sinh a_f + g_3(1)],$
$\Theta_f(1) = B_1[b_6 \cosh a_f + b_7 \sinh a_f + g_1(1)]$, $g_1(z) = B_1[\Delta_1 - \Delta_2 + \Delta_3 - \Delta_4], g_{1m}(z_m) = B_1[\Delta_5 - \Delta_6]$.

6.2. Model 2: Parabolic temperature profile: $\chi_f(z) = 2z$ and $\chi_m(z_m) = 2z_m$

Introducing model (Sparrow et al. [42]) into (40) and (44), the profile takes the form

$$\Theta_f(z) = B_1[b_{10} \cosh a_f z + b_{11} \sinh a_f z + g_4(z)]\,, \tag{58}$$

$$\Theta_m(z_m) = B_1[b_{12} \cosh a_m z_m + b_{13} \sinh a_m z_m + g_{4m}(z_m)]\,. \tag{59}$$

From (47), the TMN for the model is

$$M_{t2} = \frac{-\Lambda_1 - a_f^2 M_{S1}\Lambda_2 - a_f^2 M_{S2}\Lambda_3}{a_f^2 \Theta_f(1)}\,, \tag{60}$$

where $\Theta_f(1) = B_1[b_{10} \cosh a_f + b_{11} \sinh a_f + g_4(1)]$,

$g_4(z) = B_1[\Delta_{17} - \Delta_{18} + \Delta_{19} - \Delta_{20}], g_{4m}(z_m) = B_1[\Delta_{21} - \Delta_{22}]$.

6.3. Model 3: Inverted Parabolic temperature profile: $\chi_f(z) = 2(1-z)$ *and* $\chi_m(z_m) = 2(1-z_m)$

When model is introduced into (40) and (44), the profile becomes

$$\Theta_f(z) = B_1[b_{14} \cosh a_f z + b_{15} \sinh a_f z + g_5(z)]\,, \tag{61}$$

$$\Theta_m(z_m) = B_1[b_{16} \cosh a_m z_m + b_{17} \sinh a_m z_m + g_{5m}(z_m)]\,. \tag{62}$$

From (47), the TMN for the profile is

$$M_{t3} = \frac{-\Lambda_1 - a_f^2 M_{S1}\Lambda_2 - a_f^2 M_{S2}\Lambda_3}{a_f^2 \Theta_f(1)}\,, \tag{63}$$

where $\Theta_f(1) = B_1[b_{14} \cosh a_f + b_{15} \sinh a_f + g_5(1)]$, $g_5(z) = B_1[\Delta_{31} - \Delta_{32} + \Delta_{33} - \Delta_{34}], g_{5m}(z_m) = B_1[\Delta_{35} - \Delta_{36}]$ (See Appendix).

7. Results and discussion

The present study aims at solving exactly the problem of Marangoni convection in presence of a heat source and temperature gradients. The exact method provides useful results and also general basic temperature profiles can be readily treated with minimum mathematical computations. The graphs are plotted using MATHEMATICA version 11. The TMNs M_{t1} for model 1 as linear, M_{t2} model 2 as parabolic, and M_{t3} model 3 as inverted parabolic temperature profiles have been investigated with the object of understanding the control of convection. The depth ratio $\hat{d}$ is used to draw the limits. The effects of the parameters $\beta, R_a^*, R_{am}^*, M_{s1}, M_{s2}$ and τ_{f2} for linear, parabolic and inverted parabolic profiles on all three TMNs are depicted in Figures 2−7. The major finding is that for a given set of fixed parameter values, the inverted parabolic profile is the most stable, while the linear profile is the most unstable, as the corresponding TMNs are highest and lowest, respectively, for porous layer dominant systems, i.e., $M_{t1} \prec M_{t2} \prec M_{t3}$.

Figure 2 depicts the fluctuations of the porous parameter β on the three TMNs for linear, parabolic, and inverted temperature profiles for $\beta = 0.1, 0.5, 1, 5, 10$. The TMNs for all three profiles rise when the value of β, i.e., the permeability of the porous layer, increases. As a result, raising the porosity parameter can influence the onset of triple-diffusive convection, which is physically sensible because the fluid has more ways to travel. As a result, the system has reached a state of equilibrium. The effect of corrected internal Rayleigh numbers R_a^* and R_{am}^* on the onset of triple-diffusive convection is explained in Figures 3 and 4 respectively, for all three profiles. Negative values of these parameters indicate heat sinks, while the positive values indicate heat sources. It is evident from the figures that these parameters are effective for larger values of depth ratio, i.e., for porous layer dominant composite layer systems and the effect of R_{am}^* is drastic when compared to that of R_a^*. For a given depth ratio, the thermal Marangoni number rises as the value of these parameters rises, indicating a delay in the commencement of the onset of triple-diffusive convection, which is particularly pronounced for R_{am}^*. The effects of M_{S1} and M_{S2}, the solute1, solute2 Marangoni numbers for $M_{S1} = M_{S2} = 1, 5, 10, 25, 50$ on the onset of triple-diffusive convection is displayed in Figures 5 and 6. The TMNs drop for each of the three temperature profiles as the solute1 Marangoni number values are raised. So, the onset of triple-diffusive convection can be postponed; hence, the system can be destabilized. The system easily stabilizes if more high-solute diffusivity salts are added. However, it is clear that the solute2 Marangoni number turns the process around. Therefore, by increasing the solute2 Marangoni number, the onset of triple-diffusive convection can be postponed, stabilizing the system and helping to determine its stability features. This demonstrates that there is a third diffusing component, at which point the onset of triple-diffusive convection influences the stability of the system.

Figure 7 displays the effects of τ_{f2}, the ratio of solute2 diffusivity to thermal diffusivity fluid in the fluid layer, which is the significance of the presence of a third diffusing component, for M_{t1}, M_{t2} and M_{t3} respectively, for the values $\tau_{f2} = 0.1, 0.3, 0.5, 0.7, 0.9$. Smaller depth ratio values, or fluid layer dominating composite layer systems, have no effect on the TMNs for any of the three profiles. In a composite layer system with a porous layer as the dominating layer, the system can become unstable as τ_{f2} is increased because onset of triple-diffusive convection begins to develop more quickly. This is perfectly understandable because, in contrast to the energy stability theory, the linear stability theory specifies sufficient requirements for stability.

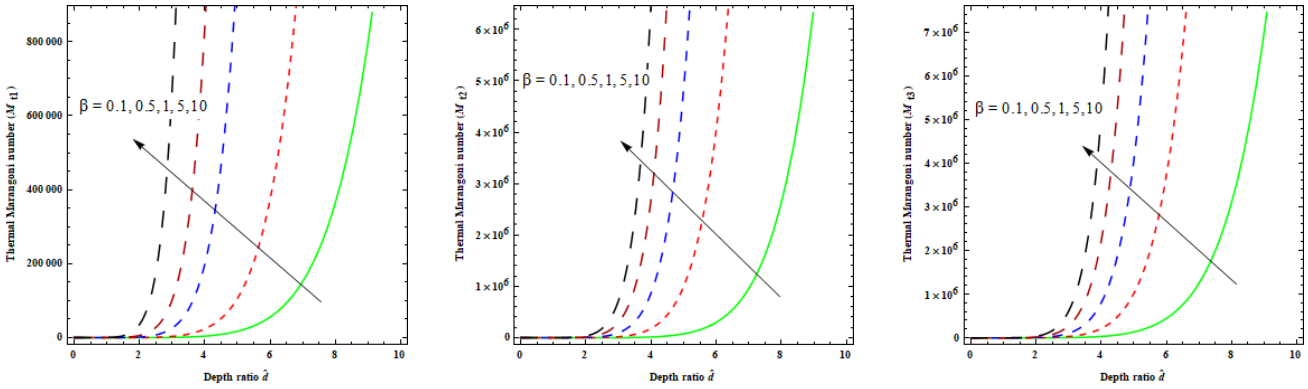

Figure 2. The effects of porous parameter β, when $\hat{T} = 0.3, a_f = 0.1, R_a^* = 1 = R_{am}^*$, $\hat{S}_1 = 0.25 = \hat{S}_2$, $\tau_{f1} = 0.25 = \tau_{f2}, \tau_{m1} = 0.5 = \tau_{m2}, M_{S1} = 10, M_{S2} = 15$.

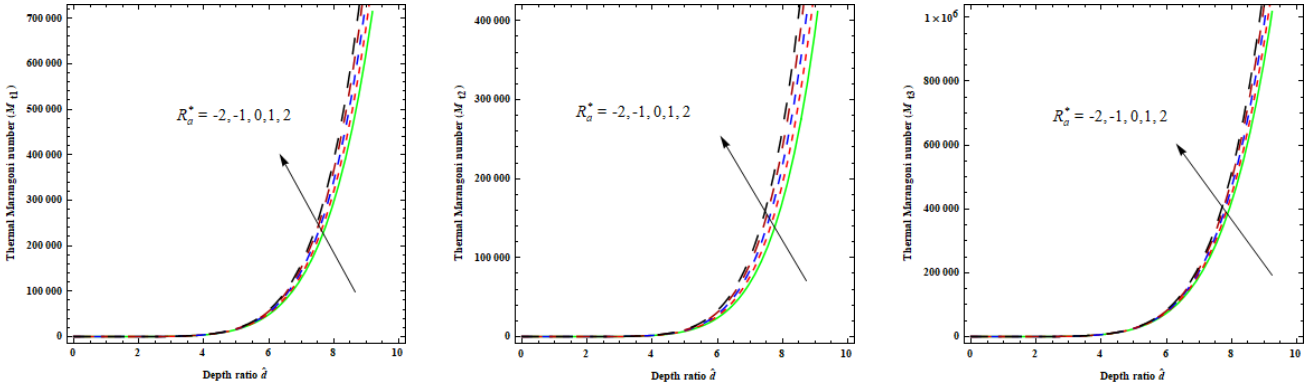

Figure 3. The effects of corrected internal Rayleigh number R_a^* for region-1, when $\hat{T} = 0.3$, $a_f = 0.1$, $\beta = 0.1, R_{am}^* = 1, \hat{S}_1 = 0.25 = \hat{S}_2, \tau_{f1} = 0.25 = \tau_{f2}, \tau_{m1} = 0.5 = \tau_{m2}, M_{S1} = 10, M_{S2} = 15$.

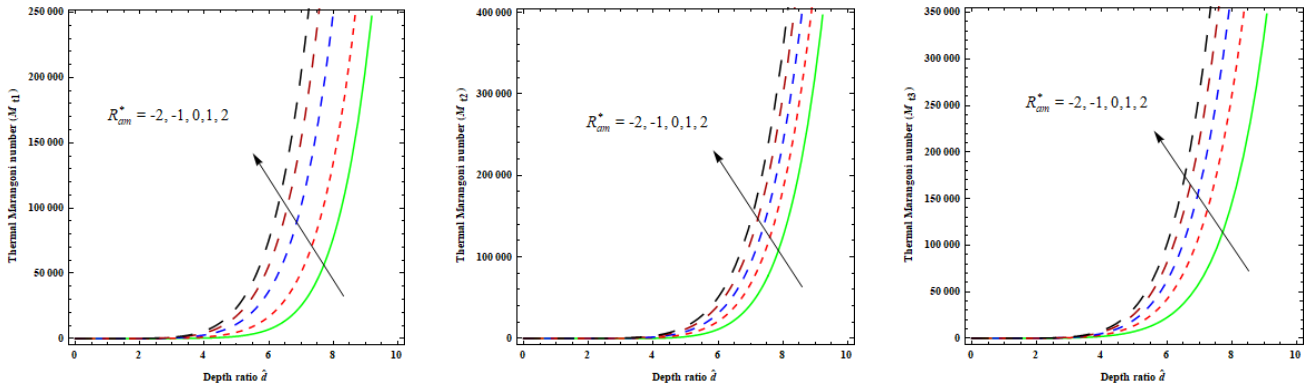

(a) (b) (c)

Figure 4. The effects of corrected internal Rayleigh number R^*_{am} for region-2, when $\hat{T} = 0.3, a_f = 0.1 = \beta, R^*_a = 1, \hat{S}_1 = 0.25 = \hat{S}_2, \tau_{f1} = 0.25 = \tau_{f2}, \tau_{m1} = 0.5 = \tau_{m2}, M_{S1} = 10, M_{S2} = 15.$

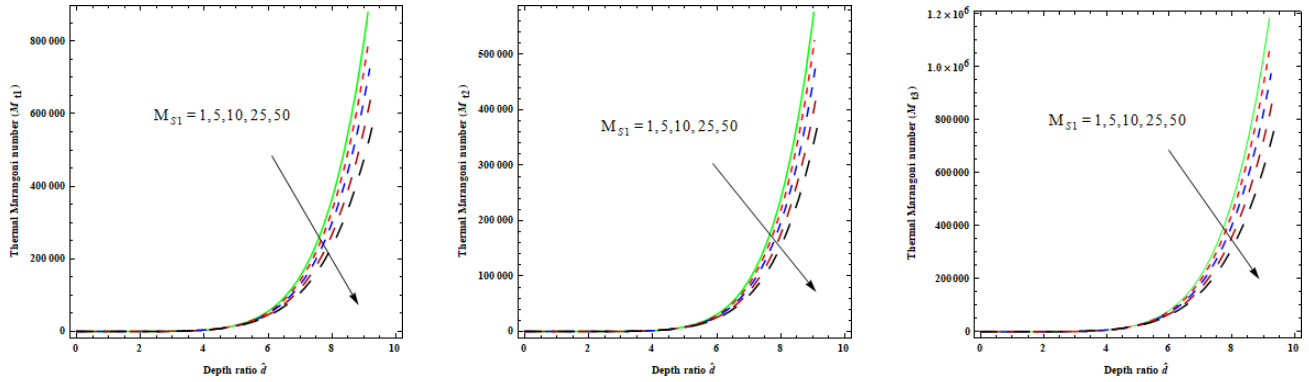

(a) (b) (c)

Figure 5. The effects of solute1 Marangoni number M_{S1} , when $\hat{T} = 0.3, a_f = 0.1 = \beta, R^*_a = 1, \ R^*_{am} = 1, \hat{S}_1 = 0.25 = \hat{S}_2, \tau_{f1} = 0.25 = \tau_{f2}, \ \tau_{m1} = 0.5 = \tau_{m2}, M_{S2} = 15.$

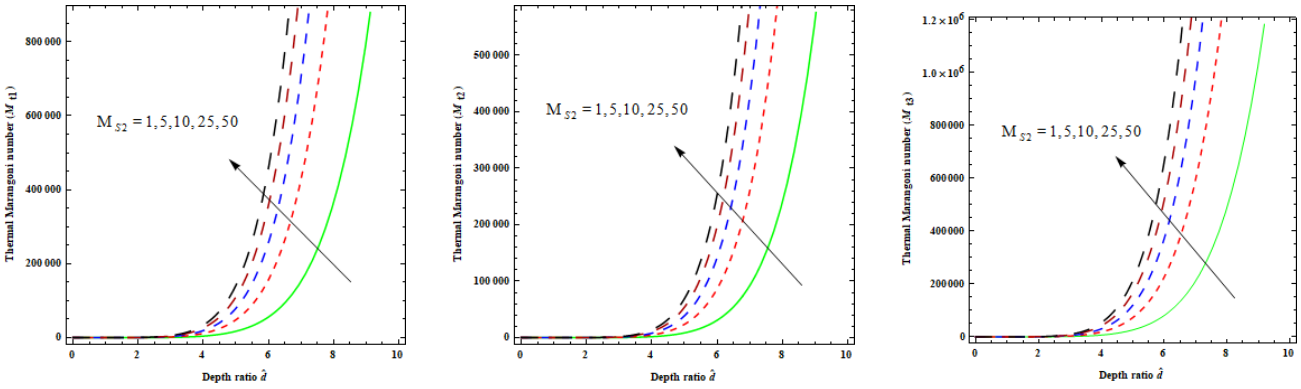

(a) (b) (c)

Figure 6. The effects of solute2 Marangoni number M_{S2}, when $\hat{T} = 0.3, a_f = 0.1 = \beta, R_a^* = 1 = R_{am}^*$, $\hat{S}_1 = 0.25 = \hat{S}_2$, $\tau_{f1} = 0.25$, $\tau_{f2} = 0.25$, $\tau_{m1} = 0.5 = \tau_{m2}, M_{S1} = 10$.

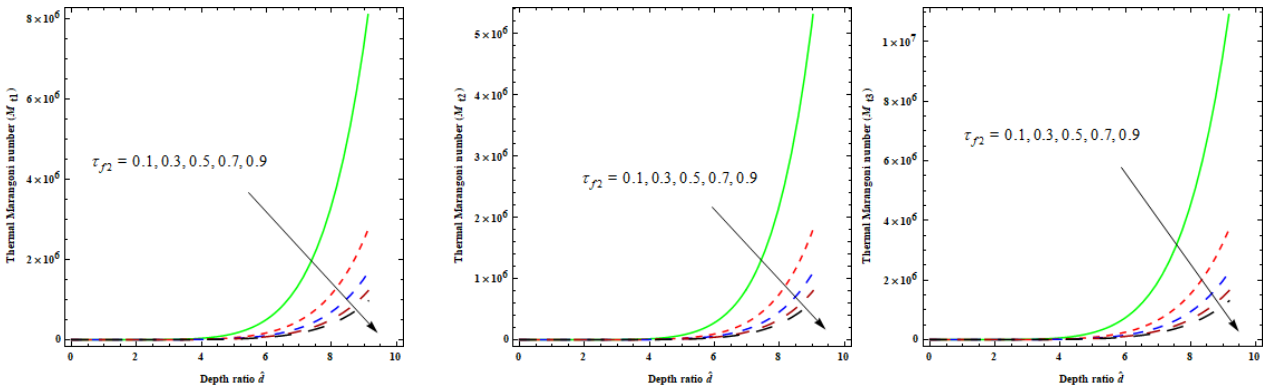

(a) (b) (c)

Figure 7. The effects of τ_{f2} in region-1, when $\hat{T} = 0.3, a_f = 0.1 = \beta, R_a^* = 1 = R_{am}^*$, $\hat{S}_1 = 0.25 = \hat{S}_2$, $\tau_{f1} = 0.25$, $\tau_{m1} = 0.5 = \tau_{m2}$, $M_{S1} = 10, M_{S2} = 15$.

8. Conclusions

The conclusions presented above provide a general framework for investigating the role of the porous parameter, corrected internal Rayleigh numbers, solutal Marangoni (surface-tension-driven) numbers, and fluid thermal diffusivity ratio on the onset of triple-diffusive convection in a fluid and fluid-saturated layer of the porous medium. For a variety of fundamental uniform and non-uniform temperature gradients in the presence of a constant heat source, the principle of exchange of stability is found to be valid, and the problem of eigenvalue is solved using the exact technique.

The investigation's findings are as follows:

- The parameters in the study have a larger influence on the porous layer dominant composite layer systems than that on the fluid layer dominant composite systems.

- ❖ The larger values of the porous parameter, corrected internal Rayleigh numbers and solute Marangoni (surface-tension-driven) number M_{s2} and the lower values of τ_{f2} and M_{s1} are preferable for controlling the onset of triple-diffusive convection.
- ❖ The system is stabilized by the porous parameter, corrected internal Rayleigh numbers, and the solute2 Marangoni (surface-tension-driven) number, while the system is destabilized by the solute1 Marangoni (surface-tension-driven) number and the ratio of the solute2 diffusivity to the thermal diffusivity of the fluid.
- ❖ The inverted parabolic temperature (model 3) profile is the most stable and hence suitable for controlling the onset of triple-diffusive convection whereas the linear temperature (model 1) profile is the most unstable for augmenting the onset of triple-diffusive convection for the set of parameters chosen for this investigation.
- ❖ The system is more stable for model 3 and less stable for model 1. i.e., $M_{t1} \prec M_{t2} \prec M_{t3}$.
- ❖ This work can be extended to temperature-dependent heat sources and Soret and Dupour effects to analyses the onset of triple-diffusive convection.

Acknowledgments

The authors are thankful for the support of Princess Nourah bint Abdulrahman University Researchers Supporting Project number (PNURSP2023R163), Princess Nourah bint Abdulrahman University, Riyadh, Saudi Arabia.

Fundings

This work was funded by Princess Nourah bint Abdulrahman University Researchers Supporting Project number (PNURSP2023R163), Princess Nourah bint Abdulrahman University, Riyadh, Saudi Arabia.

Conflict of interest

Authors are declaring no conflict of interest.

References

1. E. T. Degens, R. P. Von Herzen, H. K. Wong, W. G. Deuser, H. W. Jannasch, Lake Kivu: Structure, chemistry and biology of an east African rift lake, *Geol. Rundsch.*, **62** (1973), 245−277. https://doi.org/10.1007/BF01826830
2. R. Sumithra, Exact solution of triple diffusive Marangoni convection in a composite layer, *Inter. J. Eng. Res. Tech.*, **1** (2012), 1−13.
3. I. S. Shivakumara, S. B. Naveen Kumar, Linear and weakly nonlinear triple diffusive convection in a couple stress fluid layer, *Int. J. Heat Mass Tran.*, **68** (2014), 542−553. https://doi.org/10.1016/j.ijheatmasstransfer.2013.09.051

4. G. C. Rana, R. Chand, V. Sharma, A. Sharda, On the onset of triple-diffusive convection in a layer of nanofluid, *J. Comput. Appl. Mech.*, **47** (2016), 67−77. https://doi.org/10.22059/JCAMECH.2016.59256
5. K. R. Raghunatha, I. S. Shivakumara, B. M. Shankar, Weakly nonlinear stability analysis of triple diffusive convection in a Maxwell fluid saturated porous layer, *Appl. Math. Mech.*, **39** (2018), 153−168. https://doi.org/10.1007/s10483-018-2298-6
6. P. M. Patil, Monisha Roy, S. Roy, E. Momoniat, Triple diffusive mixed convection along a vertically moving surface, *Int. J. Heat Mass Tran.*, **117** (2018), 287−295. https://doi.org/10.1016/j.ijheatmasstransfer.2017.09.106
7. P. M. Patil, M. Roy, A. Shashikant, S. Roy, E. Momoniat, Triple diffusive mixed convection from an exponentially decreasing mainstream velocity, *Int. J. Heat Mass Tran.*, **124** (2018), 298−306. https://doi.org/10.1016/j.ijheatmasstransfer.2018.03.052
8. G. Melathil, S. Pranesh, S. Tarannum, Effects of magnetic field and internal heat generation on triple diffusive convection in an Oldroyd-B liquid, *Int. J. Res. Advent Tech.*, **7** (2019)**,** 154−163.
9. M. Archana, B. J. Gireesha, B. C. Prasannakumara, Triple diffusive flow of Casson nanofluid with buoyancy forces and nonlinear thermal radiation over a horizontal plate, *Arch. Thermodyn.*, **40** (2019), 49–69. https://doi.org/10.24425/ather.2019.128289
10. I. A. Badruddin, Azeem, T. M. Yunus Khan, M. A. Ali Baig, Heat transfer in porous media: A mini review, *Mater. Today*, **24** (2020), 1318−1321. https://doi.org/10.1016/j.matpr.2020.04.447
11. S. U. Khan, H. Vaidya, W. Chammam, S. A. Musmar, K. V. Prasad, I. Tlili, Triple diffusive unsteady flow of Eyring-Powell nanofluid over a periodically accelerated surface with variable thermal features, *Front. Phys*., **8** (2020), 246. https://doi.org/10.3389/fphy.2020.00246
12. S. Shankar, S. B. Ramakrishna, N. Gullapalli, N. Samuel, Triple diffusive MHD Casson fluid flow over a vertical wall with convective boundary conditions, *Biointerface Res. Appl. Chem.*, **11** (2021), 13765−13778. https://doi.org/10.33263/BRIAC116.1376513778
13. Y. X. Li, U. F. Alqsair, K. Ramesh, S. U. Khan, M. I. Khan, Nonlinear heat source/sink and activation energy assessment in double diffusion flow of micropolar (non-Newtonian) nanofluid with convective conditions, *Arab J. Sci. Eng*., **47** (2022), 859–866. https://doi.org/10.1007/s13369-021-05692-7
14. M. Sohail, U. Nazir, E. R. El-Zahar, H. Alrabaiah, P. Kumam, A. A. A. Mousa, et al., A study of triple-mass diffusion species and energy transfer in Carreau–Yasuda material influenced by activation energy and heat source, *Sci. Rep.*, **12** (2022), 10219. https://doi.org/10.1038/s41598-022-13890-y
15. B. K. Sharma, R. Gandhi, Combined effects of Joule heating and non-uniform heat source/sink on unsteady MHD mixed convective flow over a vertical stretching surface embedded in a Darcy-Forchheimer porous medium, *Propul. Power Res.*, **11** (2022), 276−292. https://doi.org/10.1016/j.jppr.2022.06.001
16. S. Noor Arshika, S. Tarannum, S. Pranesh, Heat and mass transfer of triple diffusive convection in viscoelastic liquids under internal heat source modulations, *Heat Tran.*, **51** (2022), 239−256. https://doi.org/10.1002/htj.22305
17. V. Nagendramma, P. Durgaprasad, N. Sivakumar, B. M. Rao, C. S. K. Raju, N. A. Shah, S. J. Yook, Dynamics of triple diffusive free convective MHD fluid flow: Lie group transformation, *Mathematics*, **10** (2022), 2456. https://doi.org/10.3390/math10142456

18. J. V. Ramana Reddy, K. Anantha Kumar, V. Sugunamma, N. Sandeep, Effect of cross diffusion on MHD non-Newtonian fluids flow past a stretching sheet with non-uniform heat source/sink: A comparative study, *Alex. Eng. J.*, **57** (2018), 1829−1838. https://doi.org/10.1016/j.aej.2017.03.008
19. B. J. Gireesha, K. Ganesh Kumar, G. K. Ramesh, B. C. Prasannakumara, Nonlinear convective heat and mass transfer of Oldroyd-B nanofluid over a stretching sheet in the presence of uniform heat source/sink, *Results Phys.*, **9** (2018), 1555−1563. https://doi.org/10.1016/j.rinp.2018.04.006
20. N. Sandeep, C. Sulochana, Momentum and heat transfer behaviour of Jeffrey, Maxwell and Oldroyd-B nanofluids past a stretching surface with non-uniform heat source/sink, *Ain Shams Eng. J.*, **9** (2018), 517−524. https://doi.org/10.1016/j.asej.2016.02.008
21. K. E. Aslani, U. S. Mahabaleshwar, P. H. Sakanaka, I. E. Sarris, Effect of partial slip and radiation on liquid film fluid flow over an unsteady porous stretching sheet with viscous dissipation and heat source/sink, *J. Porous Media*, **24** (2021), 1−15. https://doi.org/10.1615/JPorMedia.2021035873
22. R. J. Punith Gowda, R. Naveen Kumar, A. M. Jyothi, B. C. Prasannakumara, I. E. Sarris, Impact of binary chemical reaction and activation energy on heat and mass transfer of Marangoni driven boundary layer flow of a non-Newtonian nanofluid, *Processes*, **9** (2021), 702. https://doi.org/10.3390/pr9040702
23. M. Ibrahim, T. Saeed, F. Riahi Bani, S. N. Sedeh, Y. M. Chu, D. Toghraie, Two-phase analysis of heat transfer and entropy generation of water-based magnetite nanofluid flow in a circular micro tube with twisted porous blocks under a uniform magnetic field, *Powder Technol.*, **384** (2021), 522−541. https://doi.org/10.1016/j.powtec.2021.01.077
24. K. Sajjan, N. Ameer Ahammad, C. S. K. Raju, N. A. Shah, T. Botmart, Study of nonlinear thermal convection of ternary nanofluid within Darcy-Brinkman porous structure with time dependent heat source/sink, *AIMS Mathematics*, **8** (2023), 4237–4260. https://doi.org/10.3934/math.2023211
25. T. Mahesh Kumar, N. A. Shah, V. Nagendramma, P. Durgaprasad, N. Sivakumar, B. Madhusudhana Rao, et al., Linear regression of triple diffusive and dual slip flow using Lie Group transformation with and without hydro-magnetic flow, *AIMS Mathematics*, **8** (2023), 5950–5979. https://doi.org/10.3934/math.2023300
26. S. U. Mamatha, R. L. V. Renuka Devi, N. Ameer Ahammad, N. A. Shah, B. Madhusudhan Rao, C. S. K. Raju, et al., Multi-linear regression of triple diffusive convectively heated boundary layer flow with suction and injection: Lie group transformations, *Int. J. Mod. Phys. B*, **37** (2023), 2350007. https://doi.org/10.1142/S0217979223500078
27. T. Liu, Reconstruction of a permeability field with the wavelet multiscale-homotopy method for a nonlinear convection-diffusion equation, *Appl. Math. Comput.*, **275** (2016), 432–437. https://doi.org/10.1016/j.amc.2015.11.095
28. T. Liu, Porosity reconstruction based on Biot elastic model of porous media by homotopy perturbation method, *Chaos Solitons Fractals*, **158** (2022), 112007. https://doi.org/10.1016/j.chaos.2022.112007
29. N. Manjunatha, R. Sumithra, Effects of non-uniform temperature gradients on triple diffusive surface tension driven magneto convection in a composite layer, *Univer. J. Mech. Eng.*, **7** (2019), 398–410. https://doi.org/10.13189/ujme.2019.070611

30. N. Manjunatha, R. Sumithra, Triple diffusive surface tension driven convection in a composite layer in the presence of vertical magnetic field, *Int. J. Eng. Adv. Tech.*, **9** (2020), 1727–1734. https://doi.org/10.35940/ijeat.C5707.029320
31. N. Manjunatha, R. Sumithra, Effects of heat source/sink on Darcian-Bènard-Magneto-Marangoni convection in a composite layer subjected to non-uniform temperature gradients, *TWMS J. Appl. Eng. Math.*, **12** (2022), 669–684.
32. N. Manjunatha, R. Sumithra, R. K. Vanishree, Influence of constant heat source/sink on non-Darcian-Bènard double diffusive Marangoni convection in a composite layer system, *J. Appl. Math. Inform.*, **40** (2022), 99–115. https://doi.org/10.14317/jami.2022.099
33. P. Rudolph, W. Wang, K. Tsukamoto, D. Wu, Transport phenomena of crystal growth-heat and mass transfer, *AIP Conf. Proc.* **1270** (2010), 107–132. https://doi.org/10.1063/1.3476222
34. P. H. Roberts, Electrohydrodynamic convection, *Q. J. Mech. Appl. Math.*, **22** (1969), 211–220. https://doi.org/10.1093/qjmam/22.2.211
35. M. I. Char, K. T. Chiang, Boundary effects on the Bènard-Marangoni instability under an electric field, *Appl. Sci. Res.*, **52** (1994), 331–354. https://doi.org/10.1007/BF00936836
36. J. A. Del Rio, S. Whitaker, Electrohydrodynamics in porous media, *Transp. Porous Media*, **440** (2001), 385–405. https://doi.org/10.1023/A:1010762226382
37. M. I. Othman, Electrohydrodynamic instability of a rotating layer of a viscoelastic fluid heated from below, *Z. Angew. Math. Phys.*, **55** (2004), 468–482. https://doi.org/10.1007/s00033-003-1156-2
38. I. S. Shivakumara, N. Rudraiah, C. E. Nanjundappa., Effect of non-uniform basic temperature gradient on Rayleigh-Bènard-Marangoni convection in ferrofluids, *J. Magn. Magn. Mater.*, **248** (2002), 379–395. https://doi.org/10.1016/S0304-8853(02)00151-8
39. I. S. Shivakumara, S. Suma, K. B. Chavaraddi, Onset of surface tension driven convection in superposed layers of fluid and saturated porous medium, *Arch. Mech.*, **58** (2006), 71–92.
40. I. S. Shivakumara, S. Suresh Kumar, N. Devaraju, Effect of non-uniform temperature gradients on the onset of convection in a couple-stress fluid-saturated porous medium, *J. Appl. Fluid. Mech.*, **5** (2012), 49–55. https://doi.org/10.36884/jafm.5.01.11957
41. P. N. Kaloni, J. X. Lou, Convective instability of magnetic fluids, *Phys. Rev. E*, **70** (2004), 026313. https://doi.org/10.1103/PhysRevE.70.026313
42. E. W. Sparrow, R. J. Goldstein, V. K. Jonson, Thermal instability in a horizontal fluid layer effect of boundary conditions and non-linear temperature profile, *J. Fluid Mech.*, **18** (1964), 513–528. https://doi.org/10.1017/S0022112064000386

Supplementary (Appendix)

$$\Delta_1 = \frac{z\cosh a_f z(2\Phi_1 + \Phi_2 z)(b_1 + \tanh a_f z)}{4a_f},\ \Delta_2 = \frac{\Phi_2 z\cosh a_f z}{4a_f^2}(1 + b_1 \tanh a_f z),$$

$$\Delta_3 = \frac{z(3a_f^2 z\Phi_1 + 2a_f^2 z^2\Phi_2 + 3\Phi_2)\cosh a_f z}{12a_f^3}(b_3 + b_2 \tanh a_f z),$$

$$\Delta_4 = \frac{z\cosh a_f z(\Phi_1 + \Phi_2 z)}{4a_f^2}(b_2 + b_3 \tanh a_f z),\ \ \Delta_5 = \frac{z_m(2\Phi_{1m} + \Phi_{2m} z_m)\sinh a_m z_m}{4a_m}(b_5 \coth a_m z_m + b_4),$$

$$\Delta_6 = \frac{\Phi_{2m} z_m \sinh a_m z_m}{4a_m^2}(b_4 \coth a_m z_m + b_5),$$

$$\Phi_1 = R_a^* - 1, \Phi_2 = -2R_a^*, \Phi_{1m} = -(R_{am}^* + 1), \Phi_{2m} = -2R_{am}^*,$$

$$b_6 = b_8\hat{T}, b_7 = \frac{1}{a}(b_9 a_m + \delta_3 - \delta_2), b_8 = \frac{\delta_8}{\delta_9}, b_9 = \frac{\delta_6}{\delta_7}, \delta_1 = -B_1[\Delta_7 + \Delta_8 + \Delta_9 + \Delta_{10}],$$

$$\Delta_7 = \frac{(2a_f^2\Phi_1 + \Phi_2(a_f^2 - 1))\cosh a_f}{4a_f^2}(1 + b_1 \tanh a_f), \Delta_8 = \frac{(\Phi_2 + 2\Phi_1)\cosh a_f}{4a_f}(b_1 + \tanh a_f),$$

$$\Delta_9 = \frac{\cosh a_f[(3a_f^2 - 3)\Phi_1 + (2a_f^2 - 3)\Phi_2]}{12a_f^2}(b_2 + b_3 \tanh a_f),$$

$$\Delta_{10} = \frac{[a_f^2\Phi_1 + \Phi_2(a_f^2 + 1)]\cosh a_f}{4a_f^3}(b_3 + b_2 \tanh a_f),$$

$$\delta_2 = B_1[\frac{(2a_f^2 b_1 - a_f b_2)\Phi_1 + (b_3 - a_f)\Phi_2}{4a_f^3}], \delta_3 = B_1[\frac{2\Phi_{1m} b_5}{4a_m} - \frac{b_4\Phi_{2m}}{4a_m^2}],$$

$$\delta_4 = -B_1[\Delta_{11} + \Delta_{12}], \Delta_{11} = \left[\frac{(\Phi_{2m} - 2\Phi_{1m})a_m^2 - \Phi_{2m}}{4a_m^2}\right](b_4 \cosh a_m - b_5 \sinh a_m),$$

$$\Delta_{12} = \left(\frac{2\Phi_{1m} - \Phi_{2m}}{4a_m}\right)(b_5 \cosh a_m - b_4 \sinh a_m),$$

$$\delta_5 = \delta_1 - (\delta_3 - \delta_2)\cosh a_f, \delta_6 = \delta_4 a_f\hat{T} \sinh a_f + \delta_5 a_m \sinh a_m,$$

$$\delta_7 = a_m \cosh a_m a_f\hat{T} \sinh a_f + a_m^2 \cosh a_f \sinh a_m,$$

$$\delta_8 = \delta_4 \cosh a_f - \delta_5 \cosh a_m, \delta_9 = -a_f \cosh a_m\hat{T} \sinh a_f - a_m \cosh a_f \sinh a_m,$$

$$\mathbb{N}_0 = \frac{1}{\tau_{f1}}[\frac{1}{2}(cosh\, a_f + b_1\, sinh\, a_f) + \frac{1}{2a_f}(b_1\, cosh\, a_f + sinh\, a_f) + \mathbb{N}_{100}],$$

$$\mathbb{N}_{100} = \frac{(a_f^2 - 1)}{4a_f^2}(b_2\, cosh\, a_f + b_3\, sinh\, a_f) + \frac{1}{4a_f}(b_3\, cosh\, a_f + b_2\, sinh\, a_f),$$

$$\mathbb{N}_1 = -\frac{b_5}{2a_m\tau_{m1}}, \mathbb{N}_2 = \frac{1}{\tau_{f1}4a_f^2}\left(b_2 - 2a_f b_1\right),$$

$$\mathbb{N}_3 = -\frac{1}{2\tau_{m1}}(b_4\, cosh\, a_m - b_5\, sinh\, a_m) + \frac{1}{2a_m\tau_{m1}}(b_5\, cosh\, a_m - b_4\, sinh\, a_m),$$

$$\mathbb{N}_4 = \hat{S}_1 a_f\, sinh\, a_f,$$

$\mathbb{N}_5 = a_m \cosh a_f, \mathbb{N}_6 = \mathbb{N}_0 - (\mathbb{N}_1 - \mathbb{N}_2)\cosh a_f,$

$\mathbb{N}_7 = \frac{1}{\tau_{f2}}[\frac{1}{2}(\cosh a_f + b_1 \sinh a_f) + \frac{1}{2a_f}(b_1 \cosh a_f + \sinh a_f) + \mathbb{N}_{70}],$

$\mathbb{N}_{70} = \frac{(a_f^2-1)}{4a_f^2}(b_2 \cosh a_f + b_3 \sinh a_f) + \frac{1}{4a_f}(b_3 \cosh a_f + b_2 \sinh a_f),$

$\mathbb{N}_8 = -\frac{b_5}{2a_m\tau_{m2}}, \mathbb{N}_9 = \frac{1}{\tau_{f2}4a_f^2}\left(b_2 - 2a_f b_1\right),$

$\mathbb{N}_{10} = -\frac{1}{2\tau_{m2}}(b_4 \cosh a_m - b_5 \sinh a_m) + \frac{1}{2a_m\tau_{m2}}(b_5 \cosh a_m - b_4 \sinh a_m),$

$\mathbb{N}_{11} = \hat{S}_2 a_f \sinh a_f, \mathbb{N}_{12} = a_m \cosh a_f, \mathbb{N}_{13} = \mathbb{N}_7 - (\mathbb{N}_8 - \mathbb{N}_9)\cosh a_f,$

$$\Delta_{17} = \frac{z(2\Phi_3 + \Phi_4 z)\cosh a_f z}{4a_f}(b_1 + \tanh a_f z), \Delta_{18} = \frac{\Phi_4 z \cosh a_f z}{4a_f^2}(1 + b_1 \tanh a_f z)$$

$$\Delta_{19} = \frac{z(3a_f^2 z\Phi_3 + 2a_f^2 z^2\Phi_4 + 3\Phi_4)\cosh a_f z}{12a_f^3}(b_3 + b_2 \tanh a_f z),$$

$$\Delta_{20} = \frac{z(\Phi_3 + \Phi_4 z)\cosh a_f z}{4a_f^2}(b_2 + b_3 \tanh a_f z)\ \Delta_{21} = \frac{z_m(2\Phi_{3m} + \Phi_{4m} z_m)\sinh a_m z_m}{4a_m}(b_5 \coth a_m z_m + b_4),$$

$$\Delta_{22} = \frac{E_{4m} z_m \sinh a_m z_m}{4a_m^2}(b_4 \coth a_m z_m + b_5), \Phi_3 = R_a^*, \Phi_4 = -2(R_a^* + 1), \Phi_{3m} = -R_{am}^*, \Phi_{4m} = -2(R_{am}^* + 1),$$

$$b_{10} = b_{12}\hat{T}, b_{11} = \frac{1}{a_f}(b_{13}a_m + \delta_{12} - \delta_{11}), b_{12} = \frac{\delta_{17}}{\delta_{18}}, b_{13} = \frac{\delta_{15}}{\delta_{16}}, \delta_{10} = -B_1[\Delta_{23} + \Delta_{24} + \Delta_{25} + \Delta_{26}],$$

$$\Delta_{23} = \frac{[2a_f^2\Phi_3 + \Phi_4(a_f^2 - 1)]\cosh a_f}{4a_f^2}(1 + b_1 \tanh a_f), \qquad \Delta_{24} = \frac{(\Phi_4 + 2\Phi_3)\cosh a_f}{4a_f}(b_1 + \tanh a_f),$$

$$\Delta_{25} = \frac{[(3a_f^2 - 3)\Phi_3 + (2a_f^2 - 3)\Phi_4]\cosh a_f}{12a_f^2}(b_2 + b_3 \tanh a_f),$$

$$\Delta_{26} = \frac{[a_f^2\Phi_3 + \Phi_4(a_f^2 + 1)]\cosh a_f}{4a_f^3}(b_3 + b_2 \tanh a_f),$$

$$\delta_{11} = B_1[\frac{(2a_f^2 b_1 - a_f b_2)\Phi_3 + (b_3 - a_f)\Phi_4}{4a_f^3}], \delta_{12} = B_1[\frac{2\Phi_{3m} b_5}{4a_m} - \frac{b_4\Phi_{4m}}{4a_m^2}], \delta_{13} = -B_1[\Delta_{27} + \Delta_{28}],$$

$$\Delta_{27} = [\frac{\Phi_{4m} - 2\Phi_{3m}}{4} - \frac{\Phi_{4m}}{4a_m^2}](b_4 \cosh a_m - b_5 \sinh a_m), \qquad \Delta_{28} = \frac{(2\Phi_{3m} - \Phi_{4m})\sinh a_m}{4a_m}(b_5 \coth a_m - b_4),$$

$$\delta_{14} = \delta_{10} - (\delta_{12} - \delta_{11})\cosh a_f, \delta_{15} = \delta_{13} a_f \hat{T} \sinh a_f + \delta_{14} a_m \sinh a_m, \delta_{16} = \delta_7,$$

$$\delta_{17} = \delta_{13}\cosh a_f - \delta_{14}\cosh a_m, \delta_{18} = \delta_9,$$

$$\Delta_{31} = \frac{z(2\Phi_5 + \Phi_6 z)\cosh a_f z}{4a_f}(b_1 + \tanh a_f z), \Delta_{32} = \frac{\Phi_6 z\cosh a_f z}{4a_f^2}(1 + b_1\tanh a_f z),$$

$$\Delta_{33} = \frac{z(3a_f^2 z\Phi_5 + 2a_f^2 z^2\Phi_6 + 3\Phi_6)\cosh a_f z}{12a_f^3}(b_3 + b_2\tanh a_f z),$$

$$\Delta_{34} = \frac{z(\Phi_5 + \Phi_6 z)\cosh a_f z}{4a_f^2}(b_2 + b_3\tanh a_f z), \quad \Delta_{35} = \frac{z_m(2\Phi_{5m} + \Phi_{6m} z_m)\sinh a_m z_m}{4a_m}(b_5\coth a_m z_m + b_4),$$

$$\Delta_{36} = \frac{\Phi_{6m} z_m\sinh a_m z_m}{4a_m^2}(b_4\coth a_m z_m + b_5),$$

$$\Phi_5 = R_a^* - 2, \Phi_6 = 2(1 - R_a^*), \Phi_{5m} = -2 - R_{am}^*, \Phi_{6m} = 2(1 - R_{am}^*),$$

$$b_{14} = b_{16}\hat{T}, b_{15} = \frac{1}{a_f}(b_{17}a_m + \delta_{22} - \delta_{21}), b_{16} = \frac{\delta_{26}}{\delta_{27}}, b_{17} = \frac{\delta_{24}}{\delta_{25}}, \delta_{19} = -B_1[\Delta_{37} + \Delta_{38} + \Delta_{39} + \Delta_{40}],$$

$$\Delta_{37} = \frac{[2a_f^2\Phi_5 + \Phi_6(a_f^2 - 1)]\cosh a_f}{4a_f^2}(1 + b_1\tanh a_f), \Delta_{38} = \frac{(\Phi_6 + 2\Phi_5)\cosh a_f}{4a_f}(b_1 + \tanh a_f),$$

$$\Delta_{39} = \frac{[3(a_f^2 - 1)\Phi_5 + (2a_f^2 - 3)\Phi_6]\cosh a_f}{12a_f^2}(b_2 + b_3\tanh a_f),$$

$$\Delta_{40} = \frac{[a_f^2\Phi_5 + \Phi_6(a_f^2 + 1)]\cosh a_f}{4a_f^3}(b_3 + b_2\tanh a_f), \delta_{20} = -B_1[\Delta_{41} + \Delta_{42}],$$

$$\Delta_{41} = \frac{[(\Phi_{6m} - 2\Phi_{5m})a_m^2 - \Phi_{6m}]\sinh a_m}{4a_m^2}(b_4\coth a_m - b_5), \Delta_{42} = \frac{[2\Phi_{5m} - \Phi_{6m}]\sinh a_m}{4a_m}(b_5\coth a_m - b_4),$$

$$\delta_{21} = B_1\left[\frac{(2a_f^2 b_1 - a_f b_2)\Phi_5 + (b_3 - a_f)\Phi_6}{4a_f^3}\right], \delta_{22} = B_1\left[\frac{2\Phi_{5m} b_5 a_m - b_4\Phi_{6m}}{4a_m^2}\right],$$

$$\delta_{23} = \delta_{19} - (\delta_{22} - \delta_{21})\cosh a_f, \delta_{24} = \delta_{20} a_f\hat{T}\sinh a_f + \delta_{23} a_m\sinh a_m,$$

$$\delta_{25} = \delta_7, \delta_{26} = \delta_{20}\cosh a_f - \delta_{23}\cosh a_m, \quad \delta_{27} = \delta_9.$$